Minerals Engineering 227 (2025) 109293

Contents lists available at ScienceDirect

Minerals Engineering

journal homepage: www.elsevier.com/locate/mineng

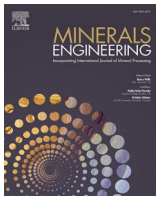

Experimental optimization of aurocyanide adsorption onto biomass activated carbon and re-examination of the adsorption mechanisms

John Kwame Bediako [a,b,*], Nicole Sharon Affrifah [b], Yeoung-Sang Yun [c], Eveliina Repo [a]

[a] Department of Separation Science, School of Engineering Science, Lappeenranta-Lahti University of Technology (LUT), FI-53850 Lappeenranta, Finland
[b] Department of Food Process Engineering, School of Engineering Sciences, College of Basic and Applied Sciences, University of Ghana, P. O. Box LG 77, Legon, Accra, Ghana
[c] Division of Semiconductor and Chemical Engineering, Jeonbuk National University, Jeonju, Jeonbuk 561-756, Republic of Korea

ARTICLE INFO

Keywords:
Biomass
KOH activation
Activated carbon
Aurocyanide
Mechanism
Ion pair

ABSTRACT

Activated carbons (ACs) prepared from agricultural residues are ideal alternatives to the commercial coal-based ACs often applied in gold mining. Carbon activation using KOH produces high-quality carbons with good textural properties. Herein, fruit peel ACs were synthesized via KOH activation and evaluated for aurocyanide adsorption. The yield and adsorption capacity were optimized through a central composite design. The Langmuir maximum equilibrium uptake was 186.95 ± 16.44 mg/g. Re-examination of the adsorption mechanisms revealed that the presence of micro and mesopores, coupled with electrostatic binding, π–π interaction and ion-pair formations influenced the significantly high adsorption capacity. This study could be useful in the syntheses and application of agro waste-derived ACs as alternative adsorbents for gold recovery from aurocyanide leachates.

1. Introduction

Activated carbon (AC) in adsorption of aurocyanide complexes has been widely applied in the extraction of gold in industrial carbon-in-pulp (CIP) and carbon-in-leach (CIL) processes, and is by far the most favorable in the long history of gold mining (Jia et al., 1998; Jia and Thomas, 2004). Although a lot of environmental issues has been raised against the use of cyanide, the cyanidation process remains the most preferred and viable option compared to other processes such as zinc precipitation and mercury amalgamation (Ibrado and Fuerstenau, 1995). In cyanidation, ores containing gold are leached with KCN or NaCN in dilute alkaline solutions in the presence of oxygen (Jia et al., 1998). Consequently, the gold is leached out from the ore in the form of $K[Au(CN)_2]$ or $Na[Au(CN)_2]$ complex and adsorbed onto the ACs that are placed on screens and flow countercurrent to the ore (Jia and Thomas, 2004; Lagerge et al., 1999; Yin et al., 2014).

The cost of commercial AC is one of the major challenges in this process, with adverse effects of raising the overall mining costs. Therefore, researchers have suggested the use of low-cost waste materials including agro waste biomass as AC precursors (Foo and Hameed, 2012; Pezoti et al., 2016; Yahya et al., 2015). Orange is one of the most favored subtropical fruits in the world (Foo and Hameed, 2012; Armando et al., 2001). With the peel occupying nearly half of the total fruit weight, it presents a good opportunity for use as an AC precursor (Foo and Hameed, 2012). Furthermore, activation using KOH is preferable owing to its lower activation temperatures, higher yields, well-defined pore size distributions, and ultrahigh specific surface areas of the resulting ACs, which can reach up to 3000 m^2/g (Yahya et al., 2015; Wang and Kaskel, 2012; Sevilla et al., 2017).

Response surface methodology (RSM) is a collection of mathematical and statistical methods useful for building empirical models and analyzing the effects of several factors (Bediako et al., 2016; Mao et al., 2011). It considers not just the factors but their interactive effects which help in optimizing the factors for higher responses. In this study, the yield and aurocyanide adsorption capacity of ACs synthesized from orange peels (OP) were optimized via a central composite design (CCD) in RSM. Factors including the activation temperature, KOH ratio and activation time were considered in the design. The responses from the CCD experiments were optimized numerically and confirmed through further experiments. Consequently, the adsorption mechanisms of aurocyanide were re-examined and elucidated.

* Corresponding author at: Department of Separation Science, School of Engineering Science, Lappeenranta-Lahti University of Technology (LUT), FI-53850 Lappeenranta, Finland.
E-mail address: john.bediako@lut.fi (J.K. Bediako).

https://doi.org/10.1016/j.mineng.2025.109293
Received 12 August 2024; Received in revised form 4 March 2025; Accepted 1 April 2025
Available online 7 April 2025

2. Methodology

Detailed description of the materials and methods is provided in the supplementary file (S1-S6). Preliminary experiments were conducted and the experimental conditions were varied to determine the appropriate factor ranges for the CCD (S2 and Table S1). Approximately 2 g each of dried pulverized OP was pre-carbonized in an automated furnace at 400 °C for 1 h under N_2 flow and allowed to cool down to room temperature. Following the CCD, the pre-carbonized samples (OPC) were treated with KOH in the designed weight ratios for 3 h, followed by activation at the set temperatures and times under continuous N_2 supply.

The KOH ratios were calculated on weight bases from a 4 M KOH stock solution. The samples were washed with 0.1 M NaOH, rinsed with DW and oven-dried at 70 °C for 24 h. The now dried activated carbons (OPACs) were weighed and the yields were calculated. Next, ~500 mg/L of aurocyanide solution was prepared and the adsorption capacities of the ACs were evaluated. Through the CCD, numerical optimizations of the AC yield and aurocyanide adsorption capacity (response variables) were performed within Design Expert software and additional experiments were run to confirm the predicted values. For comparison of the synthesis methods, the optimized OPACs were also fabricated by a one-step carbonization and activation process.

3. Results and discussion

3.1. Characterization studies

Various techniques were employed to study the characteristics of the ACs and mechanisms of aurocyanide adsorption. Thermogravimetric analysis (TGA) and textural properties including BET surface area and pore size distribution of the pristine OP, OPC, and optimal OPAC were examined by N_2 adsorption and discussed in S7 (Figs. S1 and S2). The BET results are summarized in Table 1. Furthermore, the crystallinities of the pristine OP and OPAC were examined by XRD. The OP was marked by two distinct peaks at $2\theta = 16.2^\circ$ and 21.3°, typical of crystalline cellulose structures (Bediako et al., 2017; Bediako et al., 2015). While the skeletal structural order of the OP was not entirely destroyed after pre-carbonization and activation, a sharp graphite-like (002) peak had emerged at ~28°, *ca.* 1–1.5° shift away from the typical graphite peak position of 26.5–27° with interlayer spacing of ~0.34 nm (Fig. S3 (a)) (Teng et al., 2011; Mishra et al., 2014; Sun et al., 2008). Besides, several amorphous-like peaks appeared at higher 2θ angles. Notable among them were the weak reflections at around 39° and 43° which corresponded to the (100) and (101) planes of a graphitic-type carbon structure, and indicated that a limited degree of graphitization had occurred (Sun et al., 2008; Huang et al., 2011; Chen et al., 2010; Nekouei et al., 2016). The amorphous-like domains were due to the randomly distributed pores and edge defects in the graphite-like structures (Lagerge et al., 1999). On the contrary, the absence of characteristic gold peaks in the OPAC spectrum after adsorption was first evidence of no crystalline gold formation, which suggested that the aurocyanide complex bound to the OPAC was in the valence state of +1 rather than 0.

Furthermore, the surface of OP as viewed on an FE-SEM equipment appeared rough jelly-like and showed the presence of C and O as the main component elements with tiny amounts of K and Ca (Fig. 1 and S4). Conversely, several randomly distributed pores typical of AC were observed on the surface of OPAC. The mesopores were much visible and dominated the micropores, which only became much visible after penetration of the adsorbed aurocyanide complex. Expectedly, the elemental composition of C increased to more than 80 % after activation, whilst the composition of O decreased to about 15 %. The very small residual K peak may be due to that which was originally contained in the pristine OP or traces of intercalated K compounds from the KOH activation step. The emergence of the Au peak after adsorption (OPAC-Au) bore obvious witness to the loading of aurocyanide complex into the porous structures of the OPAC. Besides, the presence of Na and Cl peaks likely arose from residuals of the base and acid used in controlling the pH; however, this may also suggest that the aurocyanide was adsorbed in its paired form with sodium (Adams et al., 1987; Adams et al., 1987; Adams, 1992).

In addition, the functional groups were studied by FTIR via the KBr disk technique as discussed in S7 (Fig. S3). To confirm the types of bonds present and binding mechanisms of the aurocyanide complex, the atomic valence and bonding states of C, N, O, K, Na and Au were analyzed. The average atomic weight percentages of the scanned elements were comparable to those obtained from the EDX analysis, though with minor discrepancies (Table S2). High resolution core-level spectra scanning of the elemental regions revealed that the surface of OPAC was composed of several chemical species as established by the preceding FTIR analysis. According to the C1s core-level spectra, four regions representing different carbon moieties, i.e., C—H (284.49 eV, 14 %), C—C/C═C (284.61 eV, 46 %), C—O/C—N (286.33 eV, 20 %) and C═O/O—C═O (289.12 eV, 11 %), and another denoting π–π* excitation at 293.34 eV (9 %) were present (Fig. 2(a)) (Valle-Vigon et al., 2013; Dementjev et al., 2000; Choi et al., 2013). The π–π* excitation peak signified formation of delocalized π conjugation of the graphene sheets in the graphite-like structures (Choi et al., 2013; Tang et al., 2015). Generally, significant amounts of oxygen and nitrogen functional groups exist at the defect sites of the non-basal planes of graphite, and these were proven in the graphite-like OPAC (Bediako et al., 2024). That is, separation of the O1s spectra before and after adsorption showed the presence of O—C═O (531.0 eV), C═O (532.0 eV) and C—O (533.01 eV) bonds (Fig. 2(b), Table S3).

Furthermore, deconvolution of the high resolution N1s spectra (Fig. S5(a)) produced peaks representative of pyridinic-N (398.29 eV, 21 %), amino-N (399.37 eV, 13 %), pyrrolic-N (400.3 eV, 22 %) and graphitic-N (401.47 eV, 45 %) (Valle-Vigon et al., 2013; Bediako et al., 2024). The pyrrolic-N and graphitic-N peaks appeared to have merged after adsorption; likely due to oxidation at the edges of the carbon crystallites resulting from loss of hydrogen atoms. In addition, the π–π* excitation peak seen in the OPAC spectrum disappeared (or was likely shielded) after adsorption, possibly due to weak donation of π-electrons from the OPAC to gold in aurocyanide complex (Ibrado and Fuerstenau, 1995). Finally, evidence of K which could be attributed to that contained in the pristine biomass or trace K compounds formed from the KOH activation was detected prior to adsorption and was completely eliminated after adsorption (Fig. S5(b)).

Table 1
N_2 uptake, BET surface area and total pore volumes of the samples.

Sample	N_2 uptake (cm^3 (STP)/g)	BET surface area (m^2/g)	Total pore volume (cm^3/g)
OP	0.45	5.53	0.060
OPC	103.78	476.96	0.326
OPAC	252.45	1098.80	0.637
OPAC-Au	224.63	986.15	0.602

3.2. Mechanisms of aurocyanide adsorption

There have been several postulates regarding the nature and mechanism of aurocyanide adsorption onto ACs. The adsorption mechanisms are of ardent interest because a better understanding of the mechanisms would essentially translate into advances in the design, synthesis and selection of ACs for the commercial cyanidation process (Yin et al., 2014). Some earlier workers have postulated the mechanisms as being dependent on the concentration and characteristics of 'spectator' cations, i.e., M^{n+}: Na^+, K^+, H^+, Ca^{2+} etc. (Adams et al., 1987; Adams et al., 1987; Adams, 1992; Davidson, 1974). Depending on the concentration

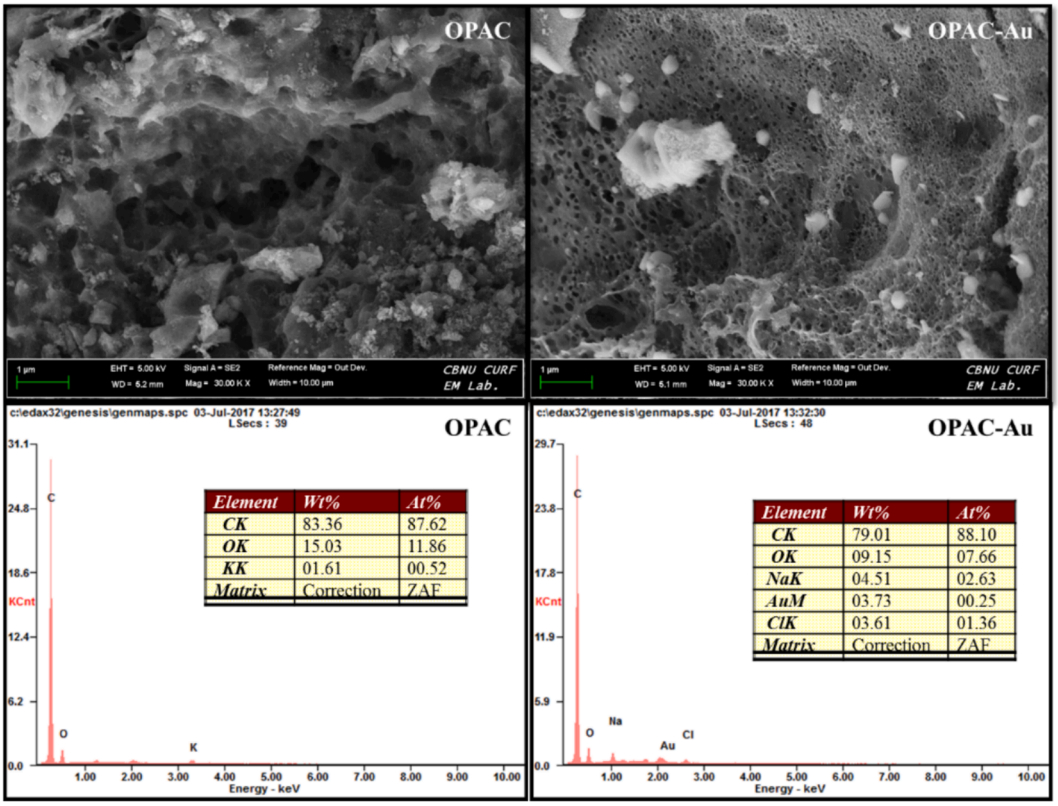

Fig. 1. FE-SEM and EDX peaks before (OPAC) and after (OPAC-Au) adsorption.

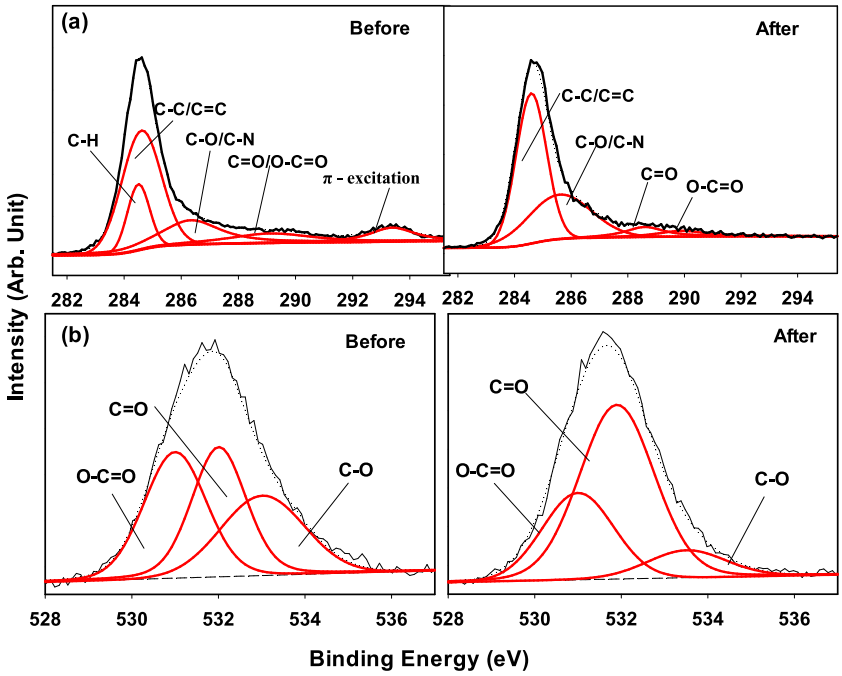

Fig. 2. (a) C1s and (b) O1s spectra of OPAC before and after adsorption.

and pH of the adsorption medium, an ion-pair of $[M^{n+}]$ $[Au(CN)_2^-]_n$ is supposedly formed between the $Au(CN)_2^-$ anion and M^{n+} cation, which is then adsorbed onto the AC (Adams et al., 1987; Adams et al., 1987; Adams, 1992). It is however important to know that the characteristics of the surface functional groups; be it negatively, positively or neutrally charged, may equally play important roles in the adsorption mechanism. That is, although adsorption of the $Na[(Au(CN)_2)]$ ion-pair was possible, a combination of other mechanisms, including electrostatic interaction between the charged sites of the AC and the $Au(CN)_2^-$ complex was equally expected as shown in Scheme 1, particularly considering the dominant presence of oxygen and nitrogen functional groups on the surface of the OPACs. Although there may be competition from OH^- in

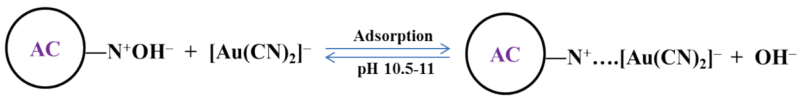

Scheme 1. Proposed electrostatic binding between charged AC and aurocyanide ion.

the strongly alkaline environment, the adsorption of $Au(CN)_2^-$ is much more favored (Yin et al., 2014; Tsuchida and Muir, 1986). Moreover, adhesion of the linear aurocyanide complex onto the graphitic planes via the π bonds was highly possible (Klauber, 1991; Jones et al., 1988; Van Deventer and Van Der Merwe, 1993), which probably led to the observed shielding of the π–excitation band found prior to adsorption.

The mechanisms of aurocyanide adsorption onto the OPACs are therefore suggested as involving a complex combination of electrostatic binding, π–π interaction and ion-pair formation, which consequently migrated into the porous structures and held by van der Waals forces (Jia and Thomas, 2004; Lagerge et al., 1999; Yin et al., 2014). The Na1s core-level spectra could also provide further credence to the proposed mechanisms with the appearance of the peak at 1072.59 eV after adsorption (Fig. S6(a)). To examine the state of the adsorbed Au species, the Au4f spectra were also separated (Fig. S6(b)). Prior to the adsorption, there was no distinct Au peak, however, a pair of peaks representing $Au4f_{7/2}$ (84.85 eV) and $Au4f_{5/2}$ (88.50 eV) of the monovalent gold, Au(I) were observed after adsorption (Leus et al., 2015; Sharma et al., 2016; Wagner, 1979). The presence of only Au(I) species meant that the aurocyanide complex was adsorbed without change or further chemical reactions that would alter the valence state of the gold, and further justified the proposed adsorption mechanisms.

3.3. Data regression, model fitting and interaction effects

The CCD experimental results and corresponding responses were regressed through quadratic model fitting (Tables S4 and S5). The statistical relevance of the quadratic model was evaluated through analysis of variance (ANOVA) and the empirical relationships among the two responses, i.e., the OPAC yield and aurocyanide uptake, the independent variables, and their interaction effects are represented by Eqs. (1) and (2). Three-dimensional plots of the interactive effects of the factors on the responses are shown in Figs. S7 and S8. The numerically optimized factors and their desired responses are presented in Fig. 3 and discussed in S8.

$$\text{Yield} = 23.20 - 4.66x_1 - 0.34x_2 - 1.34x_3 - 0.44x_1x_2 - 1.19x_1x_3 + 1.19x_2x_3 - 2.37x_1^2 - 0.46x_2^2 - 0.84x_3^2 \quad (1)$$

$$\text{Uptake} = 101.66 + 15.90x_1 + 5.60x_2 + 6.62x_3 - 0.15x_1x_2 + 1.85x_1x_3 + 2.90x_2x_3 - 11.36x_1^2 - 13.43x_2^2 - 13.69x_3^2 \quad (2)$$

where x_1, x_2 and x_3 are the coded values of the independent variables, i.e., activation temperature, KOH ratio and activation time, respectively. The above equations were statistically significant at *F*-values of 20.84 and 13.81, and *p*-values (Prob > *F*) of 0.0007 and 0.0023, for the yield and uptake responses, respectively (Tables S6 and S7). These meant that there were only 0.07 % and 0.23 % chances that such large model *F*-values could be due to noise (Bediako et al., 2016). Generally, larger *F*-values and smaller *p*-values indicate higher significance of the respective coefficients of the response variable(s) (Bediako et al., 2016; Mao et al., 2011). Moreover, model terms with "Prob > *F*" values of <0.05 indicate that they are significant and those >0.1 are not significant. By these clarifications, it implied that the model terms, x_1, x_3, x_1x_3, x_2x_3 and x_1^2 were significant model terms for the yield response, however, only the x_2x_3 interaction term had a positive effect on the yield (Eq. (1)). This was though not unexpected since changes in the activation temperature and

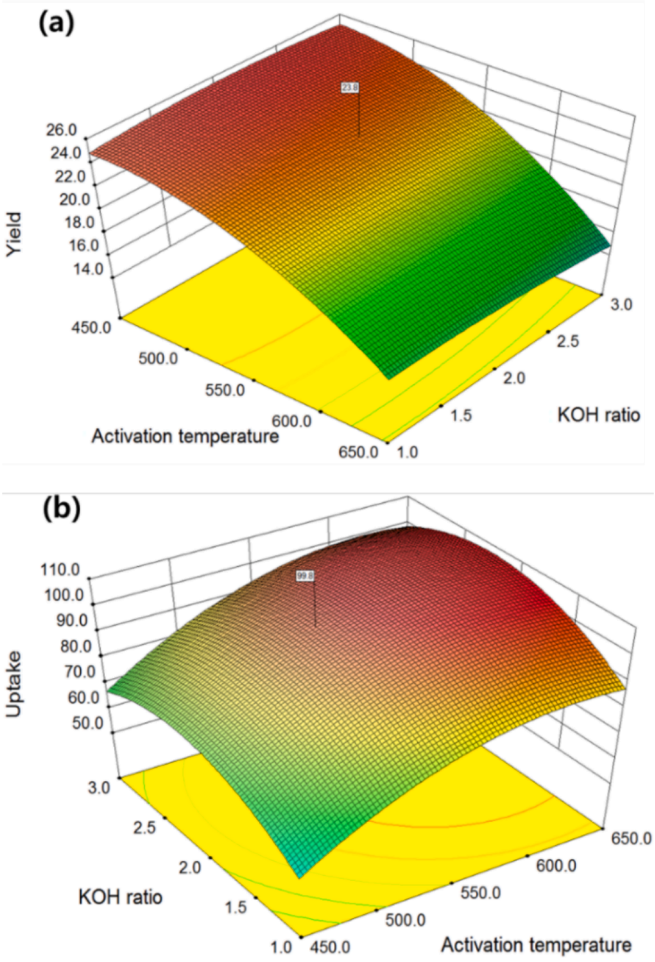

Fig. 3. Three-dimensional (3D) surface plots of numerically optimized factors and desired responses; (a) yield and (b) uptake responses.

time affect the reactivity of KOH with carbon, and hence affect the yield, i.e., higher temperature and longer time would promote effective KOH-carbon interaction and for that matter higher porosity, but less carbon yield (Table S8) (Wang and Kaskel, 2012; Otowa et al., 1993). On the other hand, the terms x_1, x_2, x_3, x_1^2, x_2^2 and x_3^2 were significant model terms for the uptake response, with x_1, x_2 and x_3 having positive influences on the uptake according to Eq. (2). This observation satisfied the KOH-carbon reactivity and porosity chemistry, i.e., possibly due to the high dependency of the adsorption capacity on the AC porosity and surface area, which are also dependent on the KOH/carbon ratio, activation temperature and activation time (Yahya et al., 2015; Foo and Hameed, 2012; Wang and Kaskel, 2012; Otowa et al., 1993). For the insignificant differences between the observed and predicted values of the yield response, a zero (0) *Pure Error* was obtained and hence the *Lack of Fit F*-value could not be defined. However, for the uptake response, an insignificant *Lack of Fit F*-value of 196.36 was observed, indicating that the model could adequately fit the data (Bediako et al., 2016).

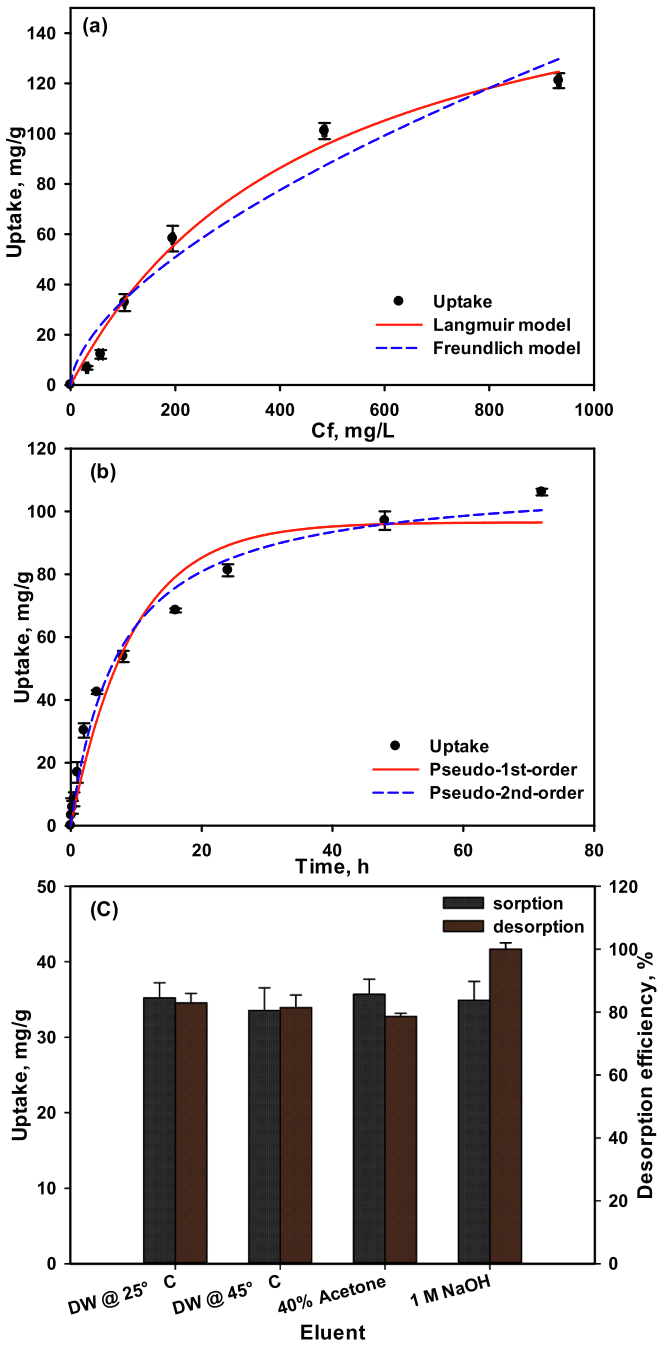

Fig. 4. (a) Isotherm and (b) kinetics of aurocyanide adsorption by OPACs and (c) adsorption–desorption using different eluents.

3.4. Batch adsorption studies

Adsorption isotherm and kinetic studies are important for setting up adsorption systems. Likewise, desorption study helps to evaluate the regeneration potential of adsorbents for commercial applications. Thus, batch isotherm, kinetic, and desorption experiments were conducted to evaluate the full performance of the optimally synthesized OPACs (Table S9). The isotherm was conducted with initial concentrations up to 1000 mg/L. The data obtained were fitted to the Langmuir and Freundlich isotherm models (Langmuir, 1918; Freundlich, 1906). According to the initial slope of the isotherm curve, the affinity of OPAC was less strong at lower concentrations, however, higher uptakes were recorded as the concentration increased (Fig. 4(a)). The isotherm curve consequently rose steadily and reached an equilibrium at higher concentrations, recording a maximum uptake of 121.08 ± 2.99 mg/g. The Langmuir model fitted the data well with coefficient of determination, R^2 value of 0.989 and a predicted maximum uptake of 186.95 ± 16.44 mg/g (Table S10). Compared to the Langmuir model, the data was less fitted to the Freundlich model, however, information on the Freundlich model's k and n values showed that an intensive binding interaction occurred between the OPACs and aurocyanide (Bediako et al., 2016).

Similarly, the adsorption kinetic experiments were conducted from 0–72 h, during which portions of the solution were timely pipetted from the bulk, centrifuged and diluted for analyses. As a common characteristic of adsorption by typical AC, the adsorption rate was quite slower to progress initially but eventually managed to approach equilibrium after a little over 20 h (Fig. 4(b)). This slow adsorption rate was likely due to the long diffusion length required for the aurocyanide complex to reach the internal pores of the OPACs (Bediako et al., 2024). To further investigate the adsorption mechanism and potential rate-controlling steps, the kinetic data was modeled with the pseudo-first- and pseudo-second-order models (Lagergren, 1898). The pseudo-first-order slightly underestimated the equilibrium uptake with R^2 value of 0.965, whilst the pseudo-second-order model predicted a slightly higher equilibrium uptake with R^2 value of 0.988, suggesting that the adsorption process followed the second order kinetics. Desorption after adsorption was attempted using DW at 25 °C and 45 °C, 40 % acetone and 1 M NaOH (Yin et al., 2014; Snyders et al., 2015; Aworn et al., 2005; Soleimani and Kaghazchi, 2008). The best eluent was 1 M NaOH, which recorded a 100 % desorption efficiency (Fig. 4(c)). There was no significant difference between the desorption efficiencies of the DW at 25 °C and 45 °C (~82 %), and the 40 % acetone was the lowest, with nearly 80 % desorption efficiency.

4. Conclusions

OPACs were synthesized via KOH activation by varying three factors; viz., KOH activation temperature, time and ratio in a CCD. Sequential pre-carbonization and activation was better than a combined single-step carbonization and activation in terms of yield. Higher temperature and longer activation time promoted effective KOH-carbon interaction and hence higher porosity and adsorption capacity but less carbon yield. Graphite-like OPACs with many C–O, C–N and π–π* excitation bonds were produced. Re-examination of the adsorption mechanisms suggested that electrostatic binding, π–π interaction and Na[$(Au(CN)_2)$] ion-pair formations played a combined role in the overall aurocyanide adsorption process. The outstanding properties and good efficiency make the OPACs an attractive alternative for application in gold recovery from gold cyanide ores.

CRediT authorship contribution statement

John Kwame Bediako: Writing – original draft, Visualization, Methodology, Investigation, Formal analysis, Data curation, Conceptualization. **Nicole Sharon Affrifah:** Writing – review & editing, Resources, Investigation, Data curation. **Yeoung-Sang Yun:** Writing – review & editing, Validation, Supervision, Resources. **Eveliina Repo:** Writing – review & editing, Supervision, Software, Project administration.

Declaration of competing interest

The authors declare the following financial interests/personal relationships which may be considered as potential competing interests: John Kwame Bediako reports financial support was provided by Research Council of Finland. If there are other authors, they declare that they have no known competing financial interests or personal relationships that could have appeared to influence the work reported in this paper.

Acknowledgements

The authors acknowledge funding support from the Research Council of Finland (decision numbers: 330076 and 358148).

Appendix A. Supplementary data

Supplementary data to this article can be found online at https://doi.org/10.1016/j.mineng.2025.109293.

Data availability

Data will be made available on request.

References

Adams, M.D., 1992. Fourier-transform infrared spectrophotometric study of adsorbed aurocyanide species on activated carbon. Hydrometallurgy 31 (1), 111–120. https://doi.org/10.1016/0304-386X(92)90111-C.

Adams, M.D., McDougall, G.J., Hancock, R.D., 1987. Models for the adsorption of aurocyanide onto activated carbon. Part III: Comparison between the extraction of aurocyanide by activated carbon, polymeric adsorbents and 1-pentanol. Hydrometallurgy 19 (1), 95–115. https://doi.org/10.1016/0304-386X(87)90044-2.

Adams, M.D., McDougall, G.J., Hancock, R.D., 1987. Models for the adsorption of aurocyanide onto activated carbon. Part II: Extraction of aurocyanide ion pairs by polymeric adsorbents. Hydrometallurgy 18 (2), 139–154. https://doi.org/10.1016/0304-386X(87)90025-9.

Armando, N., Spreen, T.H., Jauregui, C., 2001. The citrus industry of Cuba: 1994-1999. Forthcoming International Working Paper, Food and Resource Economics Department, University of Florida, Gainesville.

Aworn, A., Thiravetyan, P., Nakbanpote, W., 2005. Recovery of gold from gold slag by wood shaving fly ash. J. Colloid Interface Sci. 287 (2), 394–400. https://doi.org/10.1016/j.jcis.2005.02.048.

Bediako, J.K., Wei, W., Kim, S., Yun, Y.-S., 2015. Removal of heavy metals from aqueous phases using chemically modified waste Lyocell fiber. J. Hazard. Mater. 299, 550–561. https://doi.org/10.1016/j.jhazmat.2015.07.033.

Bediako, J.K., Wei, W., Yun, Y.-S., 2016. Low-cost renewable adsorbent developed from waste textile fabric and its application to heavy metal adsorption. J. Taiwan Inst. Chem. Eng. 63, 250–258. https://doi.org/10.1016/j.jtice.2016.03.009.

Bediako, J.K., Kim, S., Wei, W., Yun, Y.S., 2016. Adsorptive separation of Pb(II) and Cu (II) from aqueous solutions using as-prepared carboxymethylated waste Lyocell fiber. Int. J. Env. Sci. Tec. 13 (3), 875–886. https://doi.org/10.1007/s13762-015-0926-7.

Bediako, J.K., Reddy, D.H.K., Song, M.-H., Wei, W., Lin, S., Yun, Y.-S., 2017. Preparation, characterization and lead adsorption study of tripolyphosphate-modified waste Lyocell fibers. J. Env. Chem. Eng. 5 (1), 412–421. https://doi.org/10.1016/j.jece.2016.12.022.

Bediako, J.K., Kudoahor, E., Lim, C.R., Affrifah, N.S., Kim, S., Song, M.H., Repo, E., 2024. Exploring the insights and benefits of biomass-derived sulfuric acid activated carbon for selective recovery of gold from simulated waste streams. Waste Manag. 177, 135–145. https://doi.org/10.1016/j.wasman.2024.02.002.

Chen, W., Zhang, H., Huang, Y., Wang, W., 2010. A fish scale based hierarchical lamellar porous carbon material obtained using a natural template for high performance electrochemical capacitors. J. Mater. Chem. 20 (23), 4773–4775. https://doi.org/10.1039/C0JM00382D.

Choi, S., Kim, K., Nam, J., Shim, S.E., 2013. Synthesis of silica-coated graphite by enolization of polyvinylpyrrolidone and its thermal and electrical conductivity in polymer composites. Carbon 60, 254–265. https://doi.org/10.1016/j.carbon.2013.04.034.

Davidson, R.J., 1974. The mechanism of gold adsorption on activated charcoal. J. S. Afr. Inst. Min. Metall.

Dementjev, A.P., de Graaf, A., Naumkin, A.V., van de Sanden, M.C.M., Serov, A.A., 2000. X-Ray photoelectron spectroscopy reference data for identification of the C_3N_4 phase in carbon-nitrogen films. Diam. Relat. Mater. 9 (2000), 1904–1907.

Foo, K.Y., Hameed, B.H., 2012. Porous structure and adsorptive properties of pineapple peel based activated carbons prepared via microwave assisted KOH and K2CO3 activation. Micropor. and Mesopor. Mater. 148 (1), 191–195. https://doi.org/10.1016/j.micromeso.2011.08.005.

Foo, K.Y., Hameed, B.H., 2012. Preparation, characterization and evaluation of adsorptive properties of orange peel based activated carbon via microwave induced K_2CO_3 activation. Bioresour. Technol. 104, 679–686. https://doi.org/10.1016/j.biortech.2011.10.005.

Freundlich, H.M.F., 1906. Über die Adsorption in Lösungen. Z Phys. Chem. A 57, 385–470.

Huang, W., Zhang, H., Huang, Y., Wang, W., Wei, S., 2011. Hierarchical porous carbon obtained from animal bone and evaluation in electric double-layer capacitors. Carbon 49 (3), 838–843. https://doi.org/10.1016/j.carbon.2010.10.025.

Ibrado, A.S., Fuerstenau, D.W., 1995. Infrared and X-ray photoelectron spectroscopy studies on the adsorption of gold cyanide on activated carbon. Miner. Eng. 8 (4–5), 441–458. https://doi.org/10.1016/0892-6875(95)00009-F.

Jia, Y.F., Steele, C.J., Hayward, I.P., Thomas, K.M., 1998. Mechanism of adsorption of gold and silver species on activated carbons. Carbon 36 (9), 1299–1308. https://doi.org/10.1016/S0008-6223(98)00091-8.

Jia, Y., Thomas, K.M., 2004. Observation of the adsorption of $K^+Au(CN)_2^-$ ion pairs on the surface of nanoporous carbon by XANES. J. Phys. Chem. B 108 (44), 17124–17128. https://doi.org/10.1021/jp0378900.

Jones, W., Klauber, C., Linge, H.G., 1988. Randol Conf. on Gold and Silver, Perth, Australia, 1988, Randol International, Golden, CO, pp. 243–248.

Klauber, C., 1991. X-ray photoelectron spectroscopic study of the adsorption mechanism of aurocyanide onto activated carbon. Langmuir 7 (10), 2153–2159. https://doi.org/10.1021/la00058a030.

Lagerge, S., Zajac, J., Partyka, S., Groszek, A.J., 1999. Comparative study on the adsorption of cyanide gold complexes onto different carbonaceous samples: measurement of the reversibility of the process and assessment of the active surface inferred by flow microcalorimetry. Langmuir 15 (14), 4803–4811. https://doi.org/10.1021/la980243t.

Lagergren, S., 1898. Zur theorie der sogenannten adsorption gelöster stoffe. , Kungl. Svensk. Vetensk. Handl. 24 (4), 1–39.

Langmuir, I., 1918. The adsorption of gases on plane surfaces of glass, mica and platinum. J. Am. Chem. Soc. 40 (9), 1361–1403. https://doi.org/10.1021/ja02242a004.

Leus, K., Concepcion, P., Vandichel, M., Meledina, M., Grirrane, A., Esquivel, D., Turner, S., Poelman, D., Waroquier, M., Van Speybroeck, V., Van Tendeloo, G., Garcia, H., Van Der Voort, P., 2015. Au@UiO-66: a base free oxidation catalyst. RSC Adv. 5 (29), 22334–22342. https://doi.org/10.1039/C4RA16800C.

Mao, J.A., Kwak, I.S., Sathishkumar, M., Sneha, K., Yun, Y.S., 2011. Preparation of PEI-coated bacterial biosorbent in water solution: Optimization of manufacturing conditions using response surface methodology. Bioresour. Technol. 102 (2), 1462–1467. https://doi.org/10.1016/j.biortech.2010.09.088.

Mishra, S.K., Tripathi, S.N., Choudhary, V., Gupta, B.D., 2014. SPR based fibre optic ammonia gas sensor utilizing nanocomposite film of PMMA/reduced graphene oxide prepared by in situ polymerization. Sens. Actuators B 199, 190–200. https://doi.org/10.1016/j.snb.2014.03.109.

Nekouei, F., Kargarzadeh, H., Nekouei, S., Tyagi, I., Agarwal, S., Kumar Gupta, V., 2016. Preparation of nickel hydroxide nanoplates modified activated carbon for malachite green removal from solutions: kinetic, thermodynamic, isotherm and antibacterial studies. Process Saf. Environ. Prot. 102, 85–97. https://doi.org/10.1016/j.psep.2016.02.011.

Otowa, T., Tanibata, R., Itoh, M., 1993. Production and adsorption characteristics of MAXSORB: High-surface area active carbon. Gas Sep. Purif. 7 (4), 241–245. https://doi.org/10.1016/0950-4214(93)80024-Q.

Pezoti, O., Cazetta, A.L., Bedin, K.C., Souza, L.S., Martins, A.C., Silva, T.L., Santos Júnior, O.O., Visentainer, J.V., Almeida, V.C., 2016. NaOH-activated carbon of high surface area produced from guava seeds as a high-efficiency adsorbent for amoxicillin removal: Kinetic, isotherm and thermodynamic studies. Chem. Eng. J. 288, 778–788. https://doi.org/10.1016/j.cej.2015.12.042.

Sevilla, M., Ferrero, G.A., Fuertes, A.B., 2017. Beyond KOH activation for the synthesis of superactivated carbons from hydrochar. Carbon 114, 50–58. https://doi.org/10.1016/j.carbon.2016.12.010.

Sharma, A.S., Kaur, H., Shah, D., 2016. Selective oxidation of alcohols by supported gold nanoparticles: recent advances. RSC Adv. 6 (34), 28688–28727. https://doi.org/10.1039/c5ra25646a.

Snyders, C.A., Bradshaw, S.M., Akdogan, G., Eksteen, J.J., 2015. Factors affecting the elution of Pt, Pd and Au cyanide from activated carbon. Miner. Eng. 80, 14–24. https://doi.org/10.1016/j.mineng.2015.06.013.

Soleimani, M., Kaghazchi, T., 2008. Adsorption of gold ions from industrial wastewater using activated carbon derived from hard shell of apricot stones – an agricultural waste. Bioresour. Technol. 99 (13), 5374–5383. https://doi.org/10.1016/j.biortech.2007.11.021.

Sun, G., Li, X., Qu, Y., Wang, X., Yan, H., Zhang, Y., 2008. Preparation and characterization of graphite nanosheets from detonation technique. Mater. Lett. 62 (4–5), 703–706. https://doi.org/10.1016/j.matlet.2007.06.035.

Tang, D., Su, J., Yang, Q., Kong, M., Zhao, Z., Huang, Y., Liao, X., Liu, Y., 2015. Preparation of alumina-coated graphite for thermally conductive and electrically insulating epoxy composites. RSC Adv. 5 (68), 55170–55178. https://doi.org/10.1039/C5RA08010J.

Teng, C.-C., Ma, C.-C.-M., Lu, C.-H., Yang, S.-Y., Lee, S.-H., Hsiao, M.-C., Yen, M.-Y., Chiou, K.-C., Lee, T.-M., 2011. Thermal conductivity and structure of non-covalent functionalized graphene/epoxy composites. Carbon 49 (15), 5107–5116. https://doi.org/10.1016/j.carbon.2011.06.095.

Tsuchida, N., Muir, D.M., 1986. Potentiometric studies on the adsorption of $Au(CN)_2^-$ and $Ag(CN)_2^-$ onto activated carbon. Metall. Trans. B 17 (3), 523–528. https://doi.org/10.1007/bf02670218.

Valle-Vigon, P., Sevilla, M., Fuertes, A.B., 2013. Carboxyl-functionalized mesoporous silica-carbon composites as highly efficient adsorbents in liquid phase. Micropor. Mesopor. Mat. 176, 78–85. https://doi.org/10.1016/j.micromeso.2013.03.049.

Van Deventer, J.S.J., Van Der Merwe, P.F., 1993. The reversibility of adsorption of gold cyanide on activated carbon. Metall. Mater. Trans. B 24 (3), 433–440. https://doi.org/10.1007/bf02666425.

Wagner, C.D., 1979. Handbook of X-ray Photoelectron Spectroscopy: A Reference Book of Standard Data for Use in X-Ray Photoelectron Spectroscopy. Physical Electronics Division, Perkin-Elmer Corp.

Wang, J., Kaskel, S., 2012. KOH activation of carbon-based materials for energy storage. J. Mater. Chem. 22 (45), 23710–23725. https://doi.org/10.1039/C2JM34066F.

Yahya, M.A., Al-Qodah, Z., Ngah, C.W.Z., 2015. Agricultural bio-waste materials as potential sustainable precursors used for activated carbon production: a review. Renew. Sust. Energ. Rev. 46, 218–235. https://doi.org/10.1016/j.rser.2015.02.051.

Yin, C.-Y., Ng, M.-F., Saunders, M., Goh, B.-M., Senanayake, G., Sherwood, A., Hampton, M., 2014. New insights into the adsorption of aurocyanide ion on activated carbon surface: electron microscopy analysis and computational studies using fullerene-like models. Langmuir 30 (26), 7703–7709. https://doi.org/10.1021/la501191h.